Neuron, Vol. 35, 121–133, July 3, 2002, Copyright ©2002 by Cell Press

Abnormal Spine Morphology and Enhanced LTP in LIMK-1 Knockout Mice

Yanghong Meng,[1,6] Yu Zhang,[1,6] Vitali Tregoubov,[1,2] Christopher Janus,[1,3] Luis Cruz,[1] Mike Jackson,[2] Wei-Yang Lu,[2] John F. MacDonald,[2] Jay Y. Wang,[4] Douglas L. Falls,[4] and Zhengping Jia[1,2,5]

[1]Program in Brain and Behavior
The Hospital for Sick Children
555 University Avenue
Toronto, Ontario M5G 1X8
[2]Department of Physiology
University of Toronto
Toronto, Ontario M5S 1A8
[3]Center for Research in Neurodegenerative Diseases
6 Queen's Park Crescent West
Toronto, Ontario M5S 3H2
Canada
[4]Department of Biology
Emory University
Atlanta, Georgia 30322

Summary

In vitro studies indicate a role for the LIM kinase family in the regulation of cofilin phosphorylation and actin dynamics. In addition, abnormal expression of LIMK-1 is associated with Williams syndrome, a mental disorder with profound deficits in visuospatial cognition. However, the in vivo function of this family of kinases remains elusive. Using LIMK-1 knockout mice, we demonstrate a significant role for LIMK-1 in vivo in regulating cofilin and the actin cytoskeleton. Furthermore, we show that the knockout mice exhibited significant abnormalities in spine morphology and in synaptic function, including enhanced hippocampal long-term potentiation. The knockout mice also showed altered fear responses and spatial learning. These results indicate that LIMK-1 plays a critical role in dendritic spine morphogenesis and brain function.

Introduction

The actin cytoskeleton is important for many cellular processes, including cytokinesis, endocytosis, chemotaxis, and neurite outgrowth (Mitchison and Cramer, 1996). Actin remodeling may be particularly important for the establishment and structural modification of dendritic spines on which the great majority of excitatory synapses are formed in the mammalian CNS (Harris, 1999; Matus, 2000; Sorra and Harris, 2000). In addition, the actin network is directly involved in synaptic regulation at mature synapses, including hippocampal long-term potentiation (LTP), a form of synaptic plasticity considered critical to learning and memory formation (Bliss and Collingridge, 1993; Malenka and Nicoll, 1999; Smart and Halpain, 2000; Rao and Craig, 2000). However, the molecular mechanisms that regulate the actin cytoskeleton at synapses are poorly understood.

Previous studies in cultured cells have indicated that the protein kinases LIM kinase (LIMK)-1 and LIMK-2 are potent regulators of actin dynamics. They exert their effect via phosphorylating and thus inactivating the actin-depolymerization factor (ADF)/cofilin (Arber et al., 1998; Yang et al., 1998; Sumi et al., 1999). ADF/cofilin can directly bind to actin filaments and promote their disassembly (Carlier et al., 1999; Bamburg, 1999). The fact that Rac- and Rho-induced cofilin phosphorylation and reorganization of actin network can be blocked by catalytically inactive LIMK suggests that LIMK is a common downstream effector of the Rho family small GTPases (Arber et al., 1998; Yang et al., 1998; Sumi et al., 1999), which are known to regulate various signaling pathways involved in the regulation of the actin cytoskeleton (Hall, 1998). LIMK can be directly phosphorylated and activated by Rho-associated protein kinases PAK and ROCK (Edwards et al., 1999; Maekawa et al., 1999; Sumi et al., 2001).

LIMK and ADF/cofilin are widely expressed in the mammalian CNS (Bamburg and Bray, 1987; Mori et al., 1997). While LIMK-2 is expressed in all cell types, LIMK-1 is restricted to neuronal tissues and accumulates at high levels at mature synapses (Bernard et al., 1994; Mizuno et al., 1994; Proschel et al., 1995; Wang et al., 2000). In addition, LIMK-1 can directly interact with protein kinase C (PKC) and neuregulins (Kuroda et al., 1996; Wang et al., 1998), both of which are known to play a critical role in the development and function of the nervous system. Furthermore, abnormal expression of several proteins including LIMK-1 results in human Williams syndrome, a complex developmental disorder characterized by mental retardation and profound deficits in visuospatial cognition (Frangiskakis et al., 1996; Belluji et al., 1999). Therefore, it has been hypothesized that LIMK-1 is critically involved in brain function via regulation of actin dynamics.

In order to address this possibility, we have generated mutant mice deficient in the expression of LIMK-1. We showed here that the knockout mice were altered in ADF/cofilin phosphorylation and the actin cytoskeleton. These mice were also perturbed in synaptic structure and function related to the actin network. Consistent with the physiological deficits, the LIMK-1 knockout mice exhibited abnormalities in behavioral responses, including impaired fear conditioning and spatial learning. Our results represent genetic and in vivo biochemical evidence for a role of LIMK signaling in the regulation of actin dynamics and in the development and function of the mammalian CNS.

Results

Altered ADF/Cofilin (AC) Phosphorylation

The LIMK-1 knockout mice were generated by homologous recombination using R1 ES cell lines followed by aggregation (Figure 1). F1 LIMK-1$^{+/-}$ breeding gener-

[5]Correspondence: jia@sickkids.ca
[6]These authors contributed equally to this work.

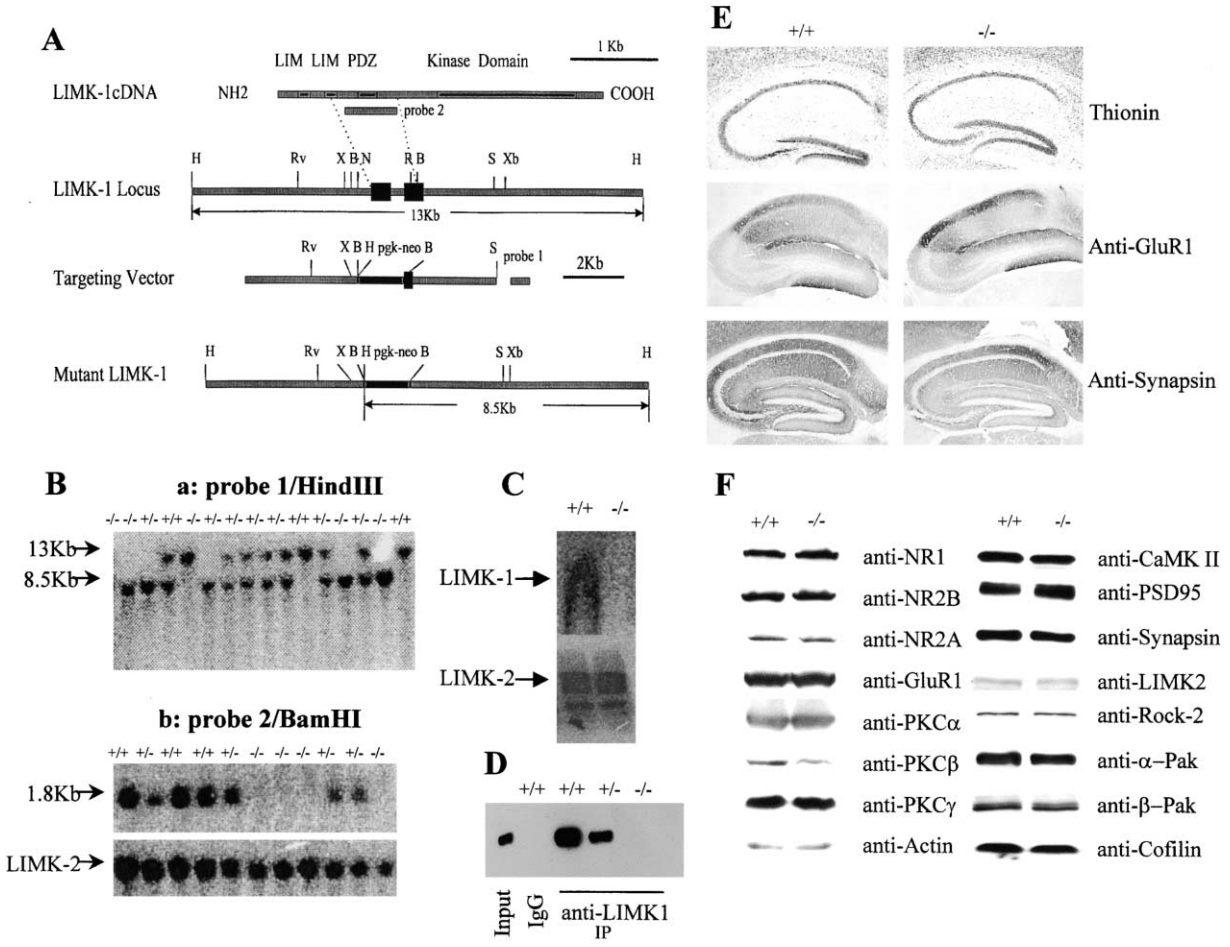

Figure 1. Targeted Disruption of LIMK-1

(A) Schematic representation of the LIMK-1 cDNA structure, the wild-type *LIMK-1* locus, the targeting vector, and the targeted *LIMK-1* locus. The solid dark boxes in the wild-type *LIMK-1* locus mark the positions of exons containing the second LIM and the PDZ domains, which have been deleted and replaced by a pgk-neo cassette in the mutant *LIMK-1* locus. H, HindIII; Rv, EcoRV; X, XhoI; B, BamHI; S, SalI; Xb, XbaI. The two probes (1 and 2) used for Southern blot analysis of ES and mouse tail DNA are indicated.

(B) Southern blot analysis of tail DNA cut either: (a) by HindIII, probed with an external probe, probe 1; or (b) by BamHI, probed with the deleted internal probe, probe 2, and with a LIMK-2 probe. Probe 1 detected a 13Kb HindIII fragment in wild-type (+/+) and heterozygous (+/−) LIMK-1 mice, and an 8.5 kb fragment in the knockout (−/−) and heterozygous mice (a). Probe 2 detected a 1.8 kb BamHI fragment only in the wild-type (+/+) and heterozygous mice (+/−), but not in the knockout mice (−/−), confirming deletion of this fragment in the targeted locus. A LIMK-2 probe detected the same pattern across all genotypes.

(C) Northern blot analysis showing an absence of LIMK-1 but normal expression of LIMK-2 mRNA in the LIMK-1 knockout mice. Total RNA was isolated from the postnatal day 7 mouse brains and hybridized with either the entire LIMK-1 cDNA or a LIMK-2 N-terminal cDNA fragment.

(D) Immunoprecipitation detection of LIMK-1 proteins. Total proteins were isolated from mature brain lysate, immunoprecipitated with either IgG or anti-LIMK-1, and detected by anti-LIMK-1. Only anti-LIMK-1 but not IgG brought down LIMK-1 in the wild-type (+/+) and heterozygous (+/−) but not in the knockout (−/−) mice. The LIMK-1 antibody was raised against the 18 C-terminal amino acids of the predicted LIMK-1 protein (Wang et al., 1998).

(E) Normal gross structure of the hippocampal formation. Paraformaldehyde-fixed and parafin-embedded brain sections were stained with either thionin or with anti-GluR1 or anti-Synapsin antibodies.

(F) Western blot analysis of various proteins. Total proteins were isolated from mature brains of wild-type (+/+) and knockout (−/−) mice and immunoblotted with the indicated antibodies.

ated an F2 population (>500 mice, 19% +/+, 51% +/−, and 30% −/−) that deviated slightly from the expected Mendelian ratio. All experiments were performed using F2 offspring of age- and sex-matched LIMK-1$^{-/-}$ (knockout) and LIMK-1$^{+/+}$ (wild-type) littermates. The knockout mice showed no detectable expression of LIMK-1 mRNA or protein (Figures 1C and 1D), but normal expression of other proteins, including LIMK-2, PAKs, ROCK 2, and cofilin (Figure 1F, n = 3). Analysis of thionin-stained 5 μm serial paraffin sections and sections labeled with anti-GluR1 and anti-synapsin antibodies revealed no significant abnormalities in gross structure of the CNS, including the hippocampus (Figure 1E), cortex, or olfactory bulb where LIMK-1 is highly expressed.

To examine the phosphorylation status of ADF/cofilin, we performed Western blot analysis on protein lysates prepared from whole-brain slices (Figure 2). While the protein levels of cofilin and ADF/cofilin were compara-

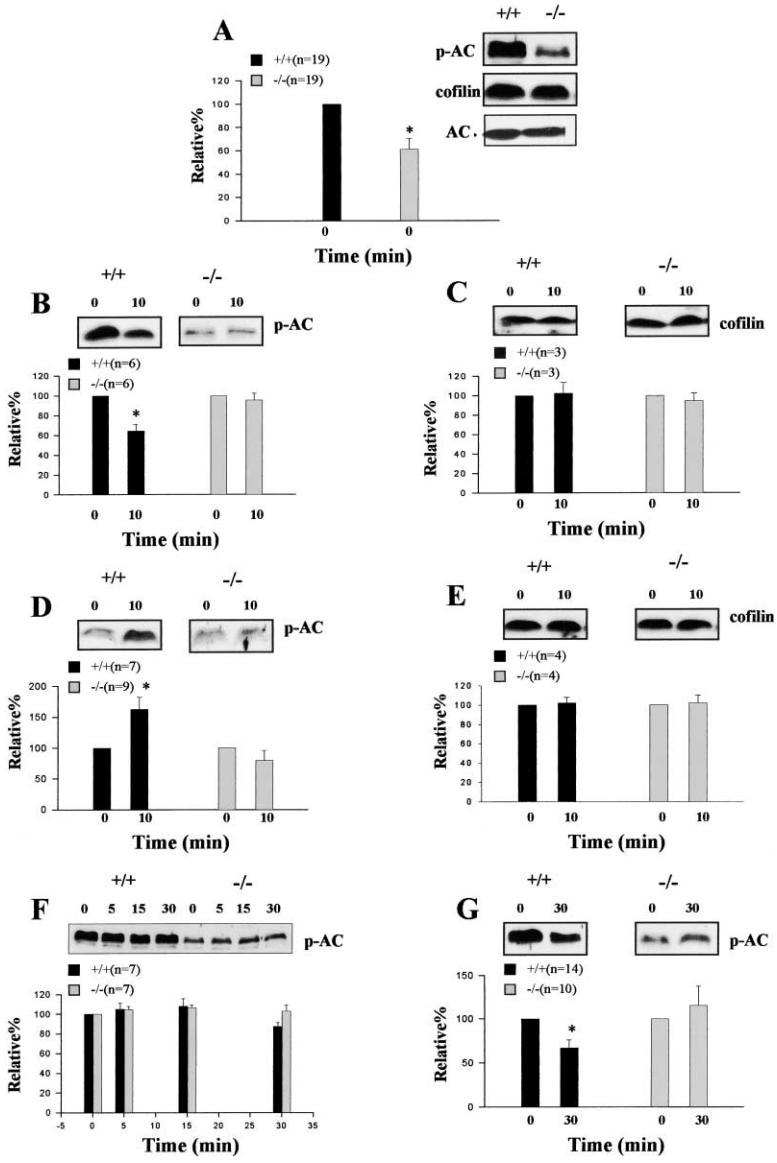

Figure 2. Altered ADF/Cofilin (AC) Phosphorylation

Western blot analysis of total cofilin, AC, and phosphorylated ADF/cofilin (p-AC) using antibodies specific to cofilin, all forms of ADF/cofilin, or p-AC.

(A) Reduction in p-AC but not the total protein level of cofilin or AC in the LIMK-1 knockout mice. The amount of p-AC in the wild-type slices was defined as 100%.

(B and C) Abolition of PDBu effect. Addition of the PKC activator PDBu (20 μM) for 10 min dramatically reduced the amount of p-AC in the wild-type but not in the knockout slices (B). The level of cofilin was not altered by the treatment with PDBu (C).

(D and E) Abolition of NMDA effect. Addition of 50 μM NMDA induced a significant increase in the amount of p-AC in wild-type but not in the knockout slices (D). Total cofilin protein was not altered by NMDA treatment in wild-type or knockout slices (E).

(F) Lack of DMSO effect. Addition of 0.1% DMSO for up to 30 min had no effect on the amount of p-AC in either wild-type or knockout slices.

(G) Abolition of glutamate effect in cultured hippocampal neurons. Addition of 100 μM glutamate for 30 min induced a significant reduction in the amount of p-AC in wild-type but not in knockout neurons. Total cofilin protein remained stable in both genotypes (data not shown). Error bars in all graphs indicate SEM. Asterisks indicate p values less than 0.05 with Student's t test. For each experiment, two slices (except four slices in [F]) from one animal of each genotype were used for treatments.

ble, the amount of phosphorylated ADF/cofilin (p-AC) was significantly lower in the knockout slices (58% ± 9% of wild-type, Figure 2A), indicating that LIMK-1 mediates, at least in part, the tonic phosphorylation of ADF/cofilin in the brain.

To evaluate the role of LIMK-1 in the regulation of p-AC in response to acute external stimuli, we assessed the effect of several agents known to alter the actin cytoskeleton in neurons. Application of 20 μM 4β-phorbol-12,13-dibutyrate (PDBu), an activator of PKC, for 10 min decreased the amount of p-AC to approximately 64% ± 6% of the untreated level in wild-type slices (Figure 2B). This rapid reduction was absent in knockout slices (treated = 96% ± 7% of untreated, Figure 2B). NMDA (50 μM) treatment for 10 min caused a significant increase in p-AC in the wild-type (163% ± 19% of untreated) but not in the knockout slices (Figure 2D). Interestingly, addition of glutamate (100 μM) for up to 30 min had no effects on brain slices (data not shown). This glutamate treatment, however, significantly reduced p-AC in cultured neurons from the wild-type (67% ± 9% of untreated) but not from the knockout mice (Figure 2G). The total protein level of cofilin was not altered by PDBu (Figure 2C), NMDA (Figure 2E), or glutamate (data not shown). Treatments with DMSO (0.1%, the maximal concentration used as vehicle for drugs) alone for 30 min did not cause any significant changes in p-AC or total cofilin in either the wild-type or knockout slices (Figure 2F). These results indicate that LIMK-1 is critical to the stimulus-induced changes in ADF/cofilin phosphorylation and/or dephosphorylation.

Abnormalities in the Actin Cytoskeleton

To directly examine if the absence of LIMK-1 affects the neuronal structures and actin cytoskeleton, we immunostained cultured hippocampal neurons for the dendritic marker MAP2, cofilin, and actin filaments. The complexity of dendritic branches, as judged by MAP2 and cofilin

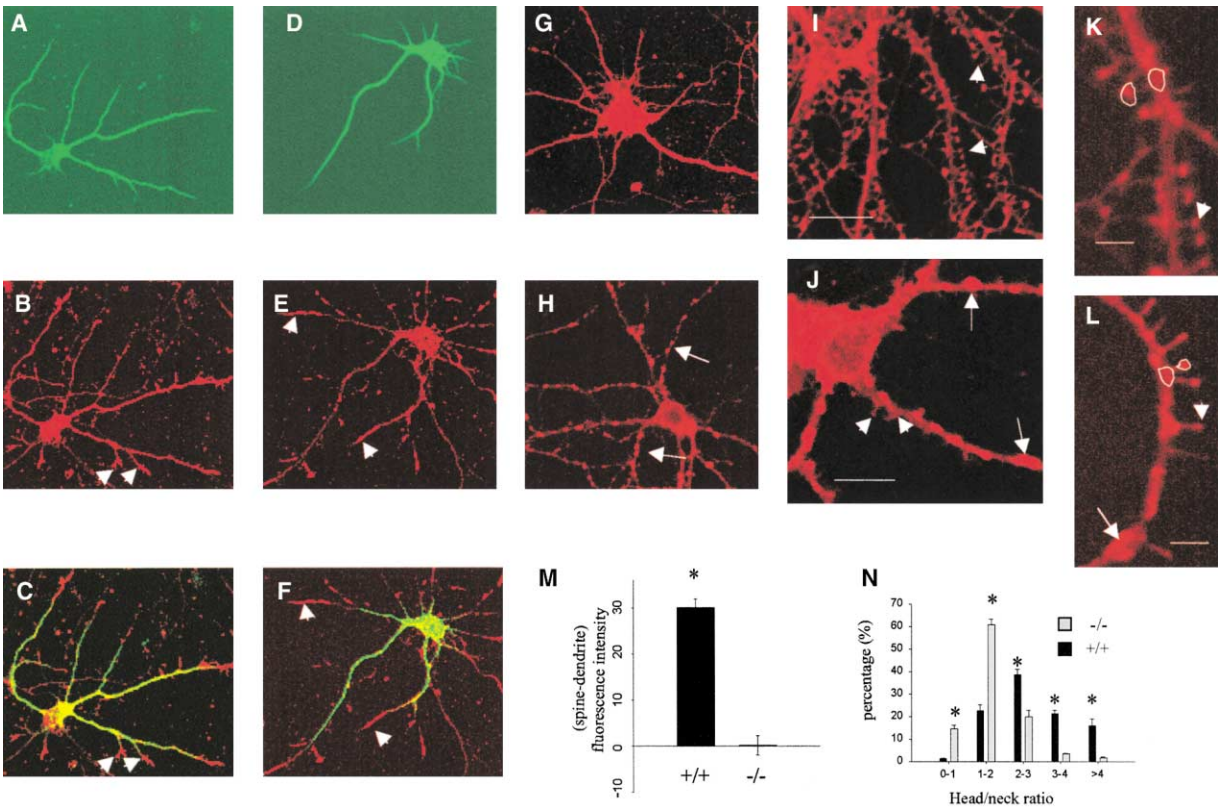

Figure 3. Abnormal Actin Cytoskeleton in the LIMK-1 Knockout Neurons

(A–F) MAP2 (A, C, D, and F) and cofilin (B, C, E, and F) double staining showing an uniform distribution of cofilin and normally spread growth cones (arrowheads) in the wild-type (A, B, and C), and an abnormal clustered distribution of cofilin and lack of growth cones (arrowheads) in the knockout (D, E, and F) hippocampal neurons (5 days in vitro).

(G and H) Phalloidin staining showing uniform distribution of actin filaments in a wild-type neuron (G) and abnormal formation of actin filament clusters (arrows) along the dendrites in a knocokout neuron (H) (8 days in vitro).

(I) Phalloidin staining of a mature wild-type neuron (17 days in vitro) showing highly enriched filamentous actin in the dendritic spines (arrowheads). Scale bar, 10 μm.

(J) Phalloidin staining of a mature knockout neuron (17 days in vitro) showing abnormal actin clusters (arrows) in the dendrites and the weakly stained spines (arrowheads). Some spines do not appear due to their weak fluorescence. Scale bar, 6 μm.

(K and L) High magnifications of phalloidin staining showing typical spines (arrowheads) of the wild-type (K) and of the knockout (L) neurons. Circles are the spine head and the corresponding dendritic area below the neck where the fluorescence intensity was measured for quantification in (M). Scale bar, 2 μm.

(M) Summary histogram of average intensity differences between spine head and the dendritic area below the neck (spine head minus dendrite fluorescence intensity $\times 10^{-3}$ gray levels of 250 spines from three independent cultures for each genotype) showing a significant difference between the wild-type and knockout neurons.

(N) Distribution of head/neck ratios of 225 randomly selected spines from three independent hippocampal cultures for each genotype. For measurements in (M) and (N), only clearly separated spines were chosen. Error bars in (M) and (N) indicate SEM. Asterisks indicate p values less than 0.05 with Student's t test.

staining, showed no differences between the wild-type and knockout neurons (Figures 3A–3F). However, the size of the growth cones was greatly reduced or completely absent in the LIMK-1 knockout neurons (Figures 3D–3F). In young neurons (5 or 8 days in vitro), both cofilin and actin were evenly distributed along the dendrites in the wild-type (Figures 3B, 3C, and 3G). In contrast, abnormal clusters of cofilin and actin were frequently observed in the knockout neurons (Figures 3E, 3F, and 3H). In mature knockout neurons (17 days), clustered actin filaments were also evident in the dendrites (Figure 3J). In the wild-type neurons (Figure 3I), the phalloidin staining intensity was much higher in spine heads compared to that in the adjacent dendritic areas where staining was low and even (average spine head/dendrite intensity ratio = 208% ± 57%; also see Figure 3M for average spine head minus dendrite intensity). In the knockout neurons (Figures 3J and 3L), the spine intensity was weak and not significantly higher than that of dendritic areas (average spine head/dendrite intensity ratio = 104% ± 21%, and Figure 3M for average spine head minus dendrite intensity). These data indicated that LIMK-1 is essential for proper accumulation and distribution of actin filaments in the dendritic branches and spines.

Abnormal Spine Morphology

Since the actin cytoskeleton is disrupted and the actin network is important for cell morphology, we suspected that the spine structures might be affected in the knock-

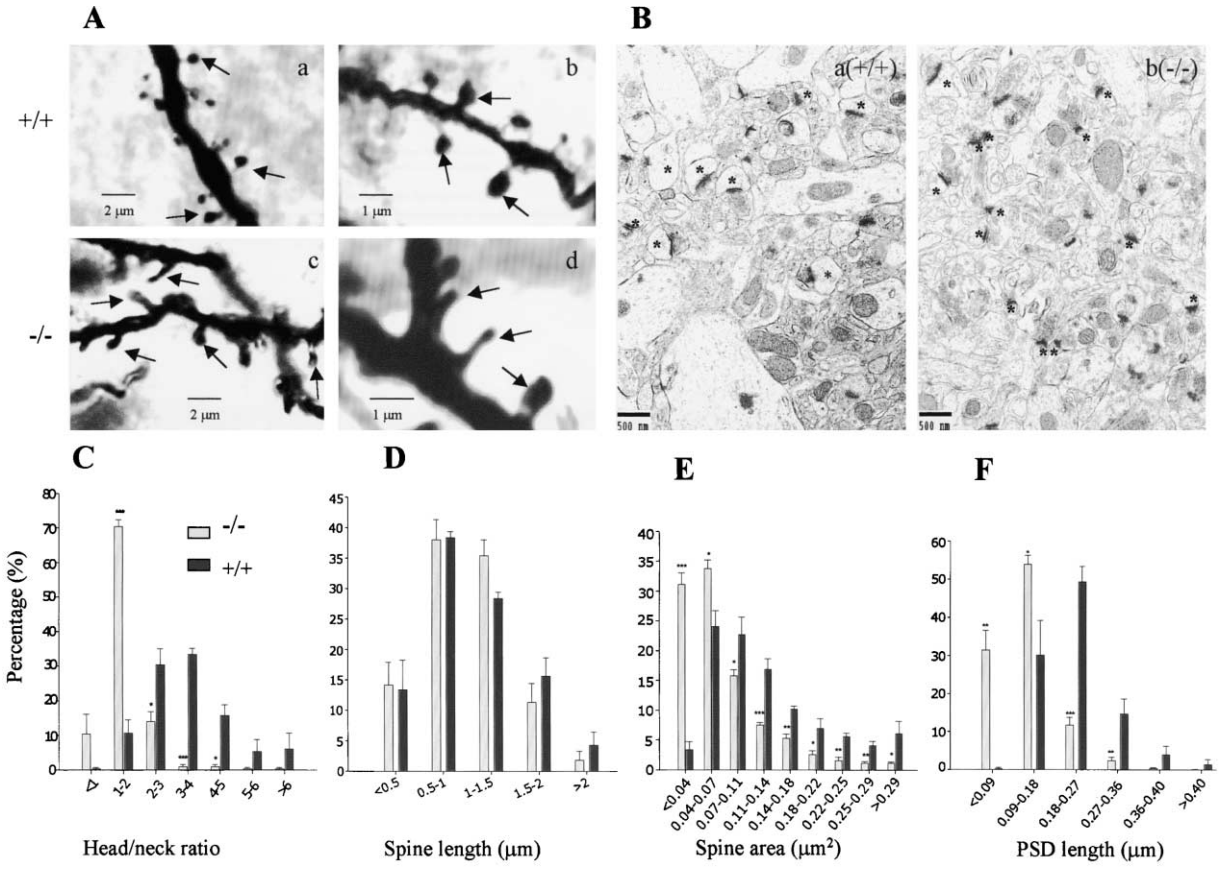

Figure 4. Abnormal Morphology of Dendritic Spines

(A) Representative single plane confocal images of Golgi-impregnated visual cortex layer V pyramidal neurons from wild-type (a and b) and knockout (c and d) mice. Arrows indicate typical dendritic spines found in both genotypes.

(B) Representative thin-section electron micrographs of hippocampal CA1 stratum radiatum from the wild-type (a) and knockout (b) mice. The cross-sectional areas and PSD lengths (asterisks) of dendritic spines bearing synapses were dramatically reduced in the knockout mice. (See supplemental data online at http://www.neuron.org/cgi/content/full/35/1/121/DC1 for larger images.)

(C and D) Distribution of head/neck ratios (C) and spine lengths (D) of randomly selected spines from the apical dendrites of layer V cortical pyramidal neurons. For each spine, the maximal diameters of the head and the neck were measured on line by adjusting the focus of the laser on a confocal microscope. A total of 300 spines from each genotype (three wild-type and three knockout adult mice) were measured.

(E and F) Distribution of cross-sectional areas (E) and postsynaptic density (PSD) lengths (F) from four wild-type and four knockout mice. For each animal, 20–35 thin-section micrographs covering neuropil regions totaling 4000–7500 μm^2 were used for quantitation. Error bars in all graphs indicate SEM. *$p < 0.05$, **$p < 0.001$, ***$p < 0.0001$ with Student's t test.

out mice. Golgi staining of rapidly fixed brain sections showed that although spine density and length were normal (Figures 4A and 4D), spine shape was clearly altered in the adult knockout mice (Figures 4A and 4C). Most dendritic spines of the pyramidal neurons of cortex and hippocampus in the wild-type mice displayed thin necks and relatively large heads, with a head/neck ratio greater than 2 (Figures 4Aa, 4Ab, and 4C), whereas most of the spines in the knockout mice had thick necks and relatively small heads, characteristic of sessile spines without a neck constriction (Figures 4Ac, 4Ad, and 4C). Almost 80% of the knockout spines had a head/neck ratio between 1 and 2, whereas fewer than 10% of the wild-type spines fell into this category (Figure 4C). The abnormal spine morphology of the knockout mice was also evident in cultured hippocampal neurons (Figures 3J, 3L, and 3N). Despite spine perturbation, EM thin sections showed that the knockout mice had a normal density of synapses identified by the presence of a distinct postsynaptic density (PSD) and presynaptic vesicles (Figure 4B). However, the cross-sectional area of the postsynaptic component of asymmetric synapses and the length of PSD of these synapses were significantly reduced in the knockout mice (Figures 4E and 4F), consistent with the results that the knockout mice had smaller spine heads in Golgi-stained sections. These results indicate that LIMK-1 is critical to establishment and/or maintenance of normal spine morphology in vivo and in culture.

Enhanced Hippocampal LTP

To investigate the physiological consequences of LIMK-1 inactivation and actin abnormalities, we performed electrophysiological recordings in the CA1 region of the hippocampus. Previous studies using actin-perturbing agents have shown that alterations of actin dynamics affect both basal synaptic transmission and hippocampal LTP (Kim and Lisman, 1999; Krucker et al.,

2000). Since basal responses were not altered in the LIMK-1 knockout mice (data not shown), we focused on analyzing hippocampal synaptic plasticity, specifically LTP and long-term depression (LTD). While LTD induced by low-frequency stimulation was normal (Figures 5A and 5E), the magnitude of LTP induced by several high-frequency stimulations was significantly altered in the knockout slices (Figure 5E). Tetanic stimulations of 5 or 10 Hz elicited LTP in the wild-type slices but failed to generate an appreciable amount of LTP in the knockout slices (Figures 5B and 5E). In contrast, LTP induced by 50 or 100 Hz stimulation was clearly enhanced in the knockout mice (Figures 5C–5E).

To investigate whether the enhanced LTP was linked to abnormal actin filaments, we analyzed the effect of the actin depolymerizing compound cytochalasin D (Cyto-D). Although it has been shown to affect both basal responses and hippocampal LTP (Kim and Lisman, 1999), low concentrations of the drug inhibit only LTP in rat hippocampus (Krucker et al., 2000). In mouse hippocampus, we found that low concentrations of Cyto-D (1 μM) actually facilitated LTP in wild-type slices. As shown in Figures 5G and 5H, bath perfusion of Cyto-D (1 μM) for 30 min with no effect on basal synaptic transmission, significantly enhanced LTP in wild-type ($p < 0.002$, Student's t test), but not in the knockout slices. Higher concentrations of Cyto-D (5 μM) again had no effect on basal responses but inhibited LTP in both genotypes although to a less degree in the knockout slices. 5 μM Cyto-D reduced LTP by 68% $\pm$ 5% in wild-type and by 44% $\pm$ 5% in knockout slices ($p < 0.02$, Student's t test, by comparing 1 μM Cyto-D and 5 μM Cyto-D LTP). Latrunculin B (0.5 μM), another actin-perturbing agent, significantly enhanced LTP in the wild-type but not in the knockout slices (data not shown). These results are consistent with the finding that there is less filamentous actin in the knockout spines, and they suggest that altered hippocampal LTP in the knockout mice is likely due to changes in the actin cytoskeleton.

Since actin-depolymerizing agents also affect distribution (Rao and Craig, 2000; Zhou et al., 2001) and channel properties of glutamate receptors (Rosenmund and Westbrook, 1993), we analyzed whole-cell synaptic currents mediated by NMDA and AMPA receptors, respectively. No differences were evident in amplitude or reversal potential (data not shown), suggesting that receptor targeting is not significantly perturbed and that altered LTP in the knockout mice is not likely caused by a differential activation of synaptic NMDA receptors during induction of LTP. However, NMDA- (Figure 5F), but not AMPA-evoked currents (data not shown) desensitize more rapidly in the knockout neurons acutely isolated from hippocampal slices. The enhanced desensitization may be linked to alterations in the actin cytoskeleton since the actin binding proteins, such as α-actinin 2, are known to interact with NMDA receptors and to affect Ca^{2+}-dependent inactivation of NMDA currents (Wyszynski et al., 1997; Krupp et al., 1999).

Faster Synaptic Depression and Increased Frequency of mEPSCs

Several studies have shown that presynaptic function is also affected by perturbations of actin dynamics (Kuromi and Kidokoro, 1998; Cole et al., 2000; Morales et al., 2000). We therefore examined if the knockout mice were altered in the properties of neurotransmitter release. The degree of paired-pulse facilitation (PPF), a short-term presynaptic plasticity, was indistinguishable between the wild-type and knockout slices (Figure 6A). The magnitude of posttetanic potentiation (PTP) was also identical between the two groups of mice (Figure 6B). When a repetitive high-frequency stimulation was applied to evoke synaptic responses, both groups showed an initial facilitation of fEPSPs followed by gradual depression as the number of stimuli increased. However, the knockout slices showed faster and increased synaptic depression (Figure 6C). The averaged fEPSPs 25 s–35 s after the onset of stimulation were 72% $\pm$ 4% and 55% $\pm$ 3% of the initial response for the wild-type and knockout mice, respectively ($p < 0.01$, Student's t test). The enhanced synaptic depression in the knockout mice suggests that LIMK-1 is involved in sustained neurotransmitter release.

Altered presynaptic function in the knockout mice was also supported by pharmacological analysis (Figures 6D and 6E). Application of aminocyclopentane-1S, 3R-dicarboxylic acid (ACPD), an agonist for metabotropic glutamate receptors, induces a transient synaptic depression that is believed to be caused by inhibition of neurotransmitter release. This depression was greatly attenuated in the knockout mice (Figure 6D). A profound change was noted in response to the PKC activator PDBu. Addition of 10 μM PDBu induced a long-lasting synaptic potentiation in wild-type slices and this potentiation was dramatically reduced in the knockout slices (Figure 6E).

To further investigate if actin filaments played a role in the alterations of neurotransmitter release, we analyzed the frequency and amplitude of miniature excitatory postsynaptic currents (mEPSCs) from CA1 pyramidal neurons. We found that, although the amplitude was not altered, the rate of mEPSCs was significantly higher in the knockout neurons (0.1–0.3 Hz for the wild-type and 0.3–0.6 Hz for the knockout neurons; Figures 6F and 6G). Addition of 10 μM Cyto-D caused a transient increase in the rate of mEPSCs in the wild-type (Figures 6H and 6I) but not in the knockout (Figure 6I) slices. The normalized frequency of mEPSCs 5 min after addition of Cyto-D was 187% $\pm$ 15% for the wild-type and 119% $\pm$ 17% for the knockout neurons ($p < 0.02$, Student's t test). Lower concentrations of Cyto-D (2 μM), latrunculin B (1 μM), or DMSO (0.1%) showed no effect in either genotype (data not shown). The enhancing effect of Cyto-D on mEPSCs and its absence in the knockout mice suggest that LIMK-1 modulates neurotransmitter release through regulating the actin cytoskeleton.

Abnormal Behavioral Characteristics

Increased Locomotor Activity in the Open-Field Test

An open-field test was used to evaluate spontaneous exploration of a new environment and locomotor activity of the mice. The knockout mice ($n = 4$) differed significantly from the wild-type mice ($n = 8$) in their overall locomotor activities [MANOVA, $F(1,10) = 10.9$, $p < 0.01$]. Univariate analyses revealed that the knockout mice

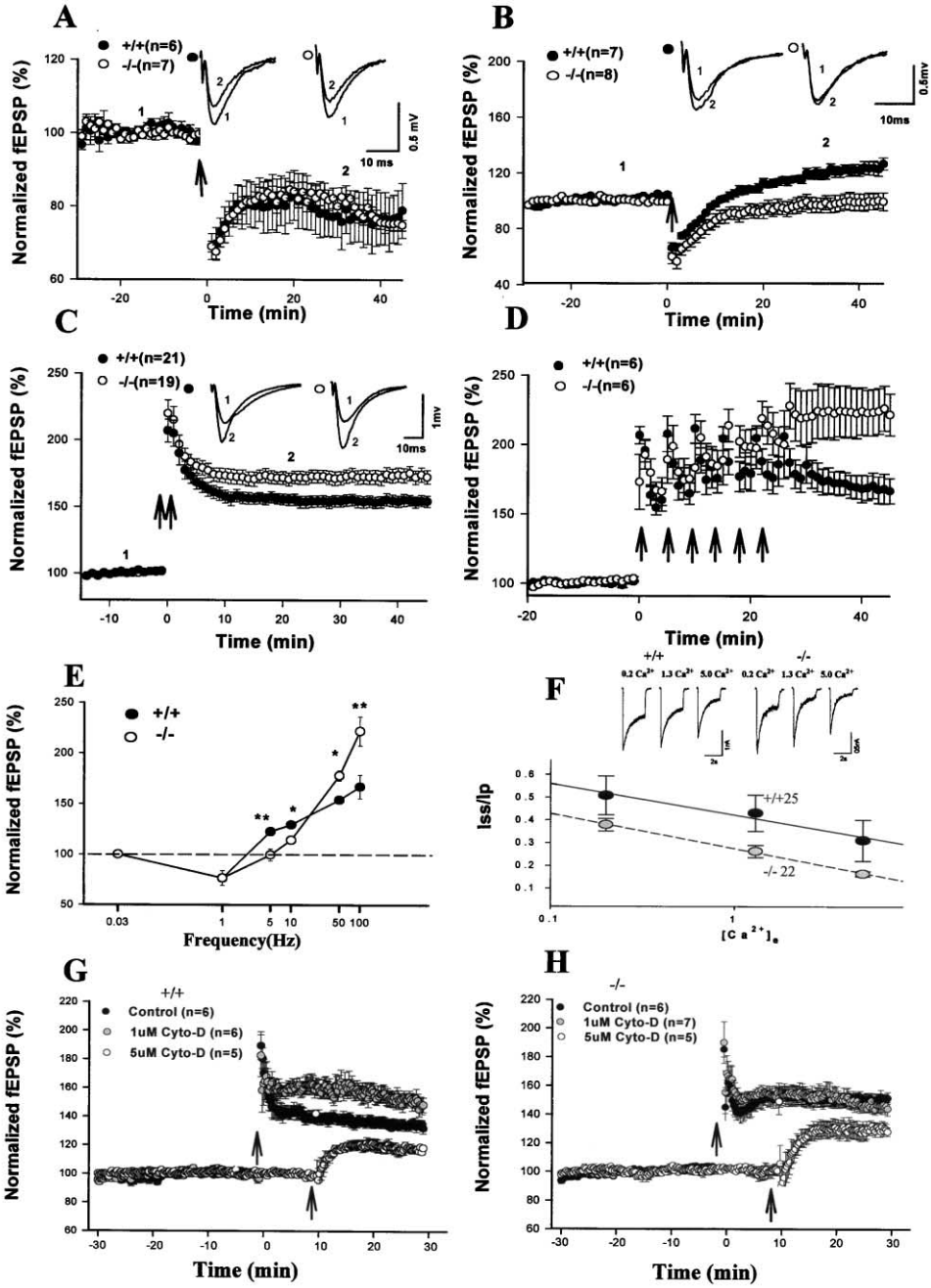

Figure 5. Altered Hippocampal LTP

(A) Normal CA1-LTD induced by 1 Hz stimulation lasting 15 min (arrow) in the knockout slices.

(B) Abolition of CA1-LTP induced by 10 Hz stimulation lasting 1.5 min (arrow) in the knockout slices.

(C) Increased CA1-LTP induced by two trains of 50 Hz stimulation (arrows, 1 s each with a 10 s intertrain interval) in the knockout mice. The magnitude of fEPSPs 30 min after the induction was 154% $\pm$ 4% for the wild-type and 178% $\pm$ 5% for the knockout slices ($p = 0.004$).

(D) Enhanced CA1-LTP induced by six trains of 100 Hz stimulation (arrows, 1 s each with 5 min intertrain interval) in the knockout mice. The fEPSP 20 min after the last train of 100 Hz stimulation was 167% $\pm$ 11% for the wild-type and 222% $\pm$ 14% for the knockout slices ($p < 0.001$).

(E) Summary plot showing alterations in the degree of LTP and LTD induced by stimulation in the CA1 area of the hippocampus at several different frequencies. *$p < 0.05$, **$p < 0.001$ with Student's t test.

(F) Enhanced desensitization of NMDA currents. Histogram of averaged steady state current (I_{ss})/peak current (I_p) ratio for 25 wild-type (+/+) and 22 knockout (−/−) neurons from four mice of each group, showing a significantly reduced I_{ss}/I_p in the knockout neurons. Above the plot are representative traces of NMDA-evoked currents in acutely isolated CA1 pyramidal neurons showing an enhanced inactivation or desensitization in the knockout neurons at various concentrations (in mM) of extracellular Ca^{2+}.

(G) Effect of Cyto-D on LTP in wild-type slices. Perfusion of 1 μM Cyto-D significantly enhanced LTP ($p < 0.002$), whereas 5 μM Cyto-D inhibited LTP ($p < 0.001$).

(H) Reduced effect of Cyto-D on LTP in the knockout slices. Perfusion of 1 μM Cyto-D had no effect on LTP although 5 μM Cyto-D decreased LTP ($p < 0.05$, Student's t test). Cyto-D was perfused during the entire experiments. LTP in (G) and (H) was induced by 1 s 100 Hz stimulation given at $t = 0$, in control and 1 μM Cyto-D, or at $t = 10$ for 5 μM Cyto-D experiments. Error bars in all graphs indicate SEM.

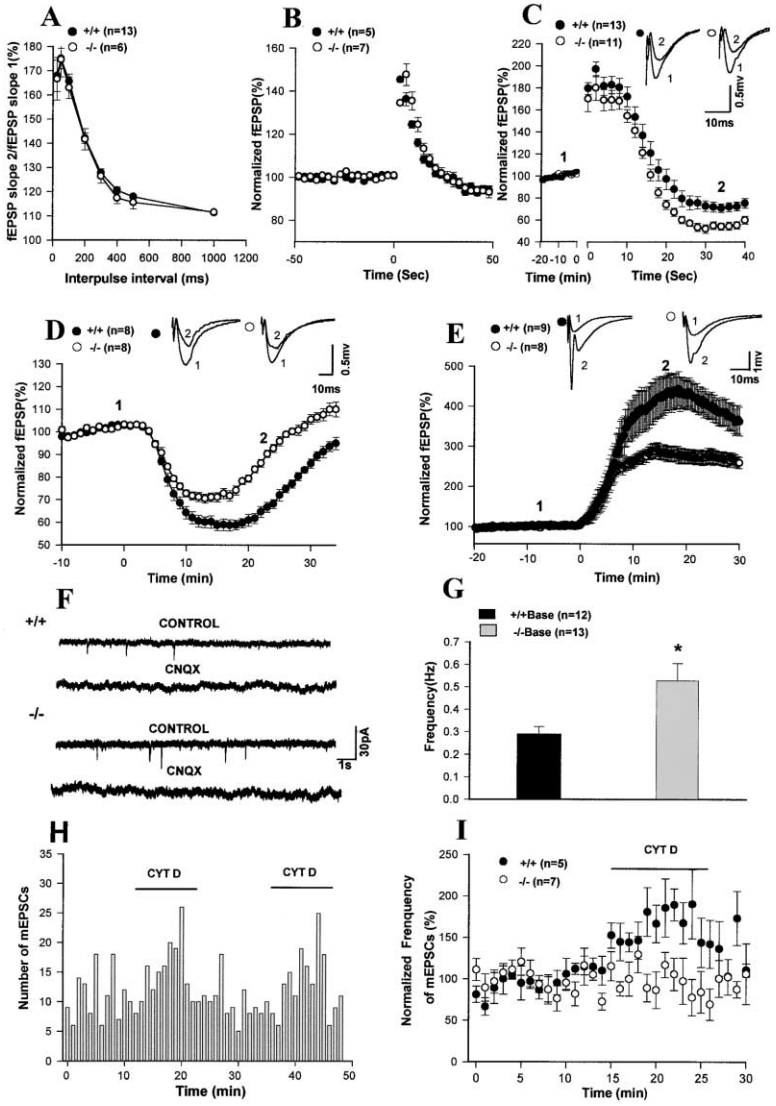

Figure 6. Altered Presynaptic Mechanisms

(A) Normal paired-pulse facilitation (PPF). The plot summarizes the ratio of the second fEPSP slope compared with the first one as a function of the interpulse interval.

(B) Normal posttetanic potentiation (PTP). A brief (1 s) 100 Hz stimulation was given at t = 0 in the presence of 50 μM D-APV, and the fEPSPs were recorded immediately after the tetanus.

(C) Faster synaptic depression in the knockout mice. Repetitive stimuli (10 Hz, lasting 40 s) were initiated at t = 0 and the fEPSP to each stimulus was recorded during this period. Each data point represents the averaged slope of 20 responses (2 s). The knockout mice showed an enhanced rate and level of depression. Above the graph are representative traces (average of four sweeps) before (1) and during (2) the 10 Hz stimulation.

(D) Reduced response to the metabotropic glutamate receptor agonist (1S, 3R)-ACPD. Application of 20 μM ACPD (at t = 0 for 10 min) resulted in a transient synaptic depression in both genotypes, but the degree of depression was significantly less in the knockout slices. Representative traces are shown above the plot.

(E) Reduced response to the phorbol ester PDBu. 10 μM PDBu was added to the perfusion solution (at t = 0 for 10 min). Representative traces (average of four sweeps) were obtained before (1) and 15 min after (2) addition of PDBu.

(F and G) Enhanced frequency of minature excitatory postsynaptic currents (mEPSCs). mEPSCs of CA1 pyramidal neurons were recorded under whole-cell voltage clamp mode in the presence of TTX (1 μM) and picrotoxin (100 μM). Representative examples (F) and summary histogram (G) showing an increased frequency of basal mEPSCs in the knockout neurons. mEPSCs were blocked by AMPA receptor antagonist CNQX (5 μM) in both wild-type and knockout neurons. Asterisks indicate p values less than 0.05 with Student's t test.

(H and I) Lack of Cyto-D effect in the knockout neurons. Representative example (H) showing an increase in the frequency of mEPSC by application of 10 μM Cyto-D in a wild-type neuron, and averaged data (I) showing differences in normalized frequency of mEPSCs between the wild-type and knockout neurons ($p < 0.02$, Student's t test). Error bars in all graphs indicate SEM.

displayed significantly higher levels of locomotor [$F(1,10) = 6.92$, $p < 0.05$] and rearing [$F(1,10) = 5.4$, $p < 0.05$] activities but not wall-leaning rate [$F(1,10) = 2.6$, $p > 0.05$] or object exploration behavior ($Fs < 1$). The elevated locomotor activity of the knockout mice was sustained during the period of testing.

Enhanced Cued Fear Response in Contextual Fear Conditioning (CFC)

To evaluate learning performance, we first employed a fear-conditioning paradigm, which provides a robust associative learning test in mice. The knockout (n = 8) and wild-type (n = 6) mice showed similar responses to different levels of a foot shock [$F(1,27) = 1.5$; Figure 7A], indicating comparable nociceptive sensitivity to aversive stimulation. Both the wild-type (n = 14) and knockout (n = 14) mice showed no freezing during the first 120 s of exploration of the conditioning chamber (Figure 7B) and comparable rates of freezing to a sound (CS phase) and to a foot shock (post-US phase) [$t(26) = 1.0$; $t(26) = 0.32$, respectively; Figure 7B]. The knockout mice also did not differ significantly from the wild-type in their freezing response during the context test carried out 24 hr later [$F(1,26) = 0.48$], though they tended to freeze more, especially in the later part of the test (Figure 7C). In the following cue-conditioning test, however, the knockout mice showed a significantly longer and constant freezing in response to the sound [$F(1,26) = 6.9$, $p < 0.02$, Figure 7D], suggesting that the fear response to simple CS stimulus is enhanced.

Impaired Learning Reversal in the Water Maze Test

In addition to CFC test, we also employed the Morris water maze test to examine more specifically spatial learning abilities of the mice. During learning acquisition training, the knockout mice (n = 8) performed comparably to the wild-type (n = 19) in search path [$F(1,25) =$

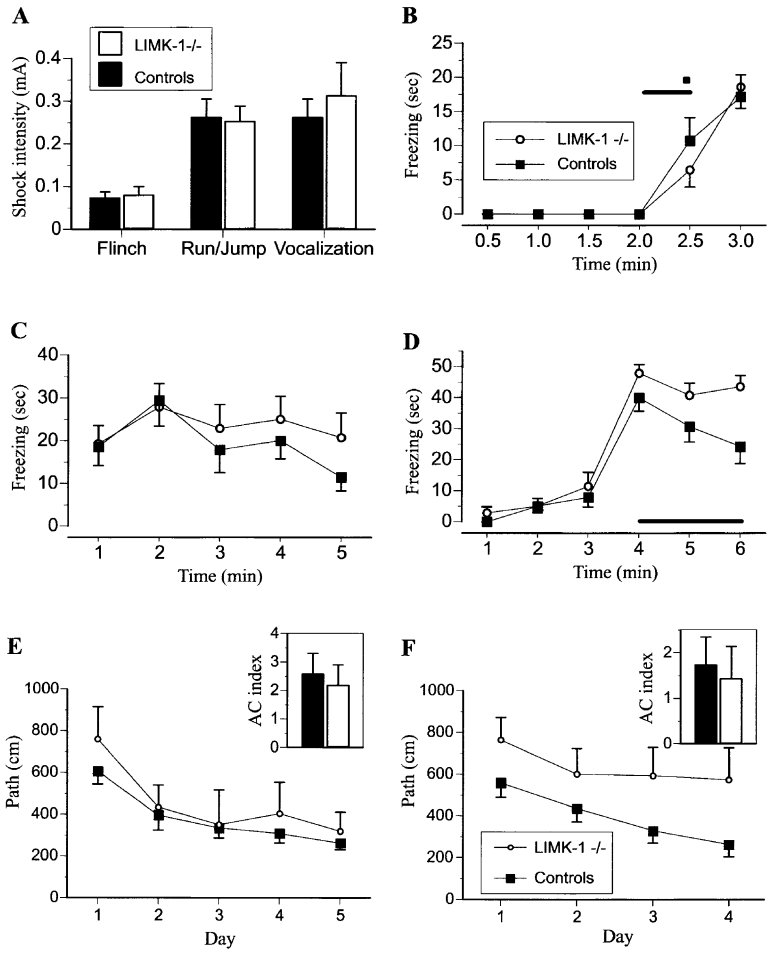

Figure 7. Altered Behavioral Responses

(A) Normal sensitivity to electric shock in the minimal amount of current required to elicit three stereotypical behavioral responses (flinching, running/jumping, and vocalizing) [$F(1,27) = 1.48$, $p = 0.23$].

(B) Freezing response to a single training trial. Solid line indicates the duration of the conditioned stimulus (CS, tone) given between the fourth and fifth 30 s interval, and the small closed square above the solid line indicates the 2 s foot shock (US). Neither knockout ($n = 14$) nor wild-type ($n = 14$) mice showed any freezing before CS onset. During the CS and after the US phase, both groups showed a similar amount of freezing (CS phase: 6.4 ± 9.3 s and 10.7 ± 12.7 s for $-/-$ and $+/+$ groups, respectively [$t(26) = 1.02$, $p = 0.32$]; post-US phase: 18.6 ± 11.7 s and 17.1 ± 12.0 s for $-/-$ and $+/+$ groups, respectively [$t(26) = 0.32$, $p = 0.75$].

(C) Contextual conditioning test 24 hr after the training trial. The knockout mice showed a slower decrease in freezing response over the testing period, although ANOVA did not show significant differences between groups [$F(1,26) = 0.48$, $p = 0.5$].

(D) Cued (CS, tone) conditioning test 2 hr after the context test. ANOVA revealed a significant group effect [$F(1,26) = 5.08$, $p < 0.05$]: the knockout mice showed more freezing and a slower decrease in freezing response. Thus, during the last minute of CS testing, the knockout mice showed a much higher freezing response [43.6 ± 3.6 s and 24.3 ± 5.5 s for $-/-$ and $+/+$, respectively; $t(26) = 2.93$, $p < 0.01$].

(E) Averaged path lengths during learning acquisition training. Both groups of mice showed a comparable initial performance [$F(1,25) = 0.73$, $p = 0.40$] and significant improvement in finding the platform over the testing period [$F(4, 100) = 10.13$, $p < 0.001$]. The insert represents an annulus crossing index (AC Index) of the spatial bias during the probe trial run 24 hr after the acquisition. Both groups showed comparable spatial bias for the platform position during the probe trail [$t(25) = 0.30$, $p = 0.8$].

(F) Averaged path lengths during the reversal of learning carried out 48 hr after the completion of the initial learning acquisition phase. The knockout mice showed a significant impairment in locating the new position of the platform [$F(1,25) = 5.0$, $p < 0.05$]. During the probe trail carried out 24 hr after the reversal training, both groups showed a comparable spatial bias for the platform position [insert; $t(25) = 0.26$, $p = 0.8$]. Error bars in all graphs indicate SEM.

0.73, Figure 7E], escape latency [$F(1,25) = 0.98$, data not shown], and swim speed [$F(1,25) = 0.02$, data not shown]. The probe trial results indicated that both groups developed similar spatial bias for the platform position site [$t(25) = 0.3$, Annulus Crossing (AC) index; Figure 7E, insert]. They did not differ in the total number of platform-site crossings [6.5 ± 1.1 and 7.2 ± 0.6 for knockout and wild-type mice, respectively, $t(25) = 0.65$], indicating comparable search patterns during the probe trial. A visible platform test carried out on experimentally naïve mice also showed no significant differences between the knockout ($n = 19$) and wild-type mice ($n = 20$) in their latency to reach the platform, swim path, or swim speed [$F(1,27) = 0.25$; $F(1,27) = 0.71$; $F(1,27) = 0.38$, respectively].

However, the knockout mice showed significant impairment in locating a submerged platform position [$F(1,25) = 5.0$, $p < 0.05$] when the platform was moved to the opposite quadrant during the learning reversal phase (Figure 7F). Although both groups improved their performance [effect of days $F(3,75) = 6.6$, $p = 0.001$; day by group interaction not significant], after the second day of learning reversal, the knockout mice did not improve their performance further (Figure 7F). This deficit was not explained by differences in their swimming speed [$F(1,25) = 1.8$]. However, both groups showed a comparable bias for the spatial position during probe trial [$t(25) = 0.26$; Figure 7F, insert]. During their search, they crossed all platform sites a comparable number of times [7.0 ± 0.8 for knockout and 6.3 ± 0.7 for wild-type mice, $t(25) = 0.55$]. These results indicate that the knockout mice are impaired in certain aspects of spatial learning performance.

Discussion

In cultured cells, LIMK-1 is a major ADF/cofilin kinase, and, through phosphorylating and thereby inhibiting ADF/cofilin, it plays an important role in regulating actin dynamics. Therefore, we hypothesized that genetic de-

letion of LIMK-1 in mice would lead to a reduction in the level of ADF/cofilin phosphorylation and an increase in its actin depolymerizing activity. Thus, we expected that in the knockout mice the actin cytoskeleleton would be altered due to the increased turnover of actin fibers and that as a consequence there would be abnormalities in the structure and function of the nervous system.

As predicted, in LIMK-1 knockout brain slices, the amount of phosphorylated ADF/cofilin is markedly diminished whereas total ADF/cofilin is unchanged (Figure 2), indicating that LIMK-1 is an important ADF/cofilin kinase in the CNS. An obvious candidate kinase responsible for the residual ADF/cofilin phosphorylation observed in the LIMK-1 knockout mice is LIMK-2, which is known to be expressed in the CNS (Mori et al., 1997) but whose expression is not altered by the absence of LIMK-1 (Figure 1). LIMK-2 is known to have activities similar to those of LIMK-1 in transfected cell lines (Smolich et al., 1997; Sumi et al., 1999). Other kinases capable of phosphorylating ADF/cofilin have been reported, but their presence in the CNS remains to be investigated (Lian et al., 2000; Toshima et al., 2001). In addition to its role in maintaining a tonic level of ADF/cofilin phosphorylation, our data revealed that LIMK-1 is critical in mediating acute effects of external stimuli, including activation of PKC and glutamate receptors. The mechanisms by which LIMK-1 affects the level of phosphorylated ADF/cofilin in the CNS have not been fully defined but may involve both protein kinases and phosphatases (Bamburg, 1999). Direct phosphorylation of ADF/cofilin by LIMK-1 has been demonstrated (Arber et al., 1998; Yang et al., 1998). LIMK-1 may also interact with other proteins such as protein phosphatases that in turn contribute to ADF/cofilin dephosphorylation (Bamburg, 1999).

In accordance with our hypothesis, we demonstrated that the actin cytoskeleton was dramatically altered by the absence of LIMK-1. In wild-type neurons, actin filaments accumulate at a much higher level in the spines compared to the dendrites. This regional accumulation is disrupted in the knockout neurons (Figure 3), indicating that LIMK-1 is critical for a high level of expression of actin filaments in the spines. Furthermore, the knockout neurons accumulate abnormal clusters of actin filaments along the dendrites. Although the molecular structure of these actin clusters remains to be determined, they may be related in some aspects to the rods previously described in rat cortical neurons treated with glutamate or by drugs that deplete ATP, treatments that also induced a reduction in phosphorylated ADF/cofilin (Minamide et al., 2000). Our results are consistent with the hypothesis that LIMK-1 is critically involved in the regulation of neuronal actin dynamics.

Dendritic spines and growth cones are actin-based structures, and therefore changes in their morphology reflect alterations in the actin cytoskeleton. In LIMK-1 knockout mice, the morphology of both spines and growth cones was altered (Figures 3 and 4), suggesting that LIMK-1 is an important regulator of the actin-based mechanisms shaping these structures. Although the molecular events that regulate spine formation and morphology are largely unknown, some important molecules have been identified (Nakayama and Luo, 2000; Ehlers, 2002). These include the Rho family of small GTPases and the postsynaptic proteins Shank, Homer, and SPAR (Luo et al., 1996; Nakayama et al.., 2000; Sala et al., 2001; Pak et al., 2001). All of these proteins can potentially regulate the actin network, and it is possible that their effects are mediated by alterations in LIMK1 activity. This possibility is supported by in vitro studies demonstrating that dominant-negative forms of LIMK-1 blocked Rac-induced cofilin phosphorylation and actin filament accumulation (Arber et al., 1998; Yang et al., 1998). While the present study has not examined the role of LIMK-1 in the regulation of actin-based spine motility, our finding that glutamate-induced changes in phosphorylated ADF/cofilin are absent in the knockout mice suggests the possibility that glutamate-induced spine motility is affected in these mice.

In the LIMK-1 knockout mice, basal synaptic transmission was normal but hippocampal LTP was altered (Figure 5). Furthermore, we found that low concentrations of the actin polymerization-inhibiting drugs Cyto-D or Latrunculin B had no effect on basal synaptic transmission but significantly increased LTP in the wild-type mice and that this facilitating effect was abolished in the knockout mice. Higher concentrations of Cyto-D (5 μM) inhibited LTP in both genotypes but to a lesser degree in the knockout mice. These results support the hypothesis that the effects of LIMK-1 on synaptic plasticity are a consequence of LIMK-1's effects on actin dynamics.

LIMK-1's regulation of spine morphology, likely through its effects on actin cytoskeleton, may be one mechanism by which LIMK-1 influences hippocampal LTP. It is thought that the main function of dendritic spines is to compartmentalize and restrict calcium and other molecules (Yuste et al., 2000). Thus, dendritic spines without neck constrictions in the knockout mice may fail to accumulate essential molecules to induce LTP when tetanic stimulations were weak (such as in the case of 5 and 10 Hz); however, under strong stimulations (such as 50 and 100 Hz), molecules such as Ca^{2+} in the activated spines may readily spread to parent dendrites and adjacent spines, inducing LTP at their synapses, thus enhancing global potentiation. Examination of spine calcium and the synapse specificity of LTP induction of the knockout mice may provide new insights into the fundamental mechanisms regulating synaptic plasticity.

The changes in spine morphology, hippocampal LTP, and NMDA receptor function in the knockout mice demonstrate essential postsynaptic functions of LIMK-1. However, our results that the knockout mice showed an enhanced synaptic depression and an increased rate of mEPSCs indicate that LIMK-1 has important presynaptic roles. The presynaptic function of LIMK-1 may also be actin-based since the facilitating effect of Cyto-D on mEPSC was abolished in the knockout mice (Figure 6), and previous studies have demonstrated a similar effect for actin polymerization inhibitors on both synaptic depression and the rate of mEPSCs (Landis et al., 1988; Cole et al., 2000; Morales et al., 2000). A role for LIMK-1 in presynaptic function is consistent with the pharmacological results that both PDBu and ACPD had an attenuated effect on synaptic transmission in the knockout mice. Early studies have indicated that these compounds exert their effect primarily through presynaptic mechanisms (Malenka et al., 1986; Finch and Jackson, 1990; Parfitt and Madison, 1993; Pin and Duvoisin, 1995). Our data suggest that synaptic regulation by PKC and

metabotropic glutamate receptors may be related to the actin cytoskeleton. This possibility is supported by the fact that LIMK-1 can physically interact with PKC (Kuroda et al., 1996) and is expressed in presynaptic terminals (Wang et al., 2000).

In addition to abnormalities in synaptic structure and function, we showed that the LIMK-1 knockout mice were altered in certain behavioral responses, including heightened locomotor activities and impaired spatial learning. Several factors, including the difficulties of the task (Morris et al., 1996) and the differences in the degree of initial learning—i.e., the knockout mice might have learned the task "better," resulting in a greater increase in the latency to locate a new platform position, may all contribute to the deficits in learning a new spatial cue. The prolonged freezing of the knockout mice in the fear response task may be related to altered habituation. Further experiments such as water maze and fear conditioning tasks with varying training intensity and testing at various posttraining time points will help to address these issues. It is important to note that the visuospatial deficits and hyperactivity are among the hallmarks of the cognitive profile of Williams syndrome patients (Belluji et al., 1999), but it remains to be determined whether the behavioral abnormalities in the knockout mice and in the human patients are related. Further behavioral analysis of the knockout mice, especially the heterozygous mice, will be important to assess if these mice can be used as a model to investigate the molecular mechanisms underlying human cognitive deficits.

Another intriguing question raised by our analysis of LIMK-1 knockout mice is whether abnormalities in dendritic spine morphology are present in Williams patients and contribute to the behavioral abnormalities observed in these patients. Spine abnormalities are commonly found in human patients suffering from neurological diseases such as Down's syndrome and Fragile X syndrome (Sorra and Harris, 2000). Fragile X knockout mice exhibit developmental stage-dependent spine abnormalities and an impairment in spatial learning resembling the spatial learning impairment observed in humans with Fragile X syndrome (Comery et al., 1997; Nimchinsky et al., 2001). These observations plus the results of this paper are consistent with the notion that alterations in spine structure may have important effects on synaptic function and behavior.

In summary, we have presented genetic and physiological evidence supporting the hypothesis that LIMK-1 is critically involved in spine morphogenesis and synaptic function via regulation of the actin cytoskeleton. Important issues for future investigation raised by this study will include determining the molecular mechanisms by which LIMK-1 regulates spine structure, synaptic function, and behavior; determining the relationship of the abnormalities observed in LIMK-1 knockout mice to the pathology of Williams syndrome; and examining effects of deleting LIMK-2 alone and in combination with LIMK-1 deletion.

Experimental Procedures

Generation of LIMK-1 Knockout Mice

A genomic clone containing the LIM and PDZ domains of the *LIMK-1* gene was isolated from a genomic 129/sv library. The targeting vector was constructed by replacing a 1.8 kb BamHI fragment containing the second LIM and PDZ domains with a pgk-neo cassette in a sense direction. The G418 resistant ES clones were tested for a targeted event by Southern blot analysis. Two probes, one external to the targeting vector upstream of LIM domain and one internal containing the PDZ domain, were used for analyzing ES cell and mouse tail DNA. The procedures for culturing and screening ES cells and for generation of chimeric mice were described previously (Jia et al., 1996).

Histochemistry, Golgi Impregnation, and Electron Microscopy

The procedures for thionin and immunostaining of fixed brain sections were described previously (Jia et al., 1996, Lu et al., 1997). For Golgi staining, brains were rapidly isolated, immersed in osmium tetroxide (0.4%)-potassium dichromate (3.0%) solution, and kept in the dark for 1 week. The fixed tissue was then rinsed with distilled water and treated further with 0.75% silver nitrate for 24 hr. The samples were then processed and paraffin embedded. Comparable sections (10–50 μm) were taken for image collection and analysis on a confocal microscope. For electron microscopy, the transcardially fixed brain samples were sliced (500 μm) on a vibratome and 1 $\times$ 1 mm CA1 areas isolated from comparable sections. The blocks were then postfixed for an additional 3 hr and processed according to standard methods. For each block, 1 μm thick sections were cut and stained with 1% toluidine blue to guide further trimming to isolate equivalent CA1 subfields. Thin sections (60 nm) were then cut and stained with uranyl acetate and Reynolds lead citrate. The number of synapses (Kirov et al., 1999) and cross-sectional areas of spines bearing synapses (Luo et al., 1996) were determined on electron micrographs at a final magnification of 25,000$\times$, using a NIH program.

Hippocampal Cell Culture, Immunostaining, and Immunoblotting

Cultured hippocampal neurons were prepared from postnatal day 1 mice and maintained according to a procedure recommended for Neurobasal-A medium (Life Technologies). Cells were typically fixed for 30 min with 4% paraformaldehyde/0.1% glutaraldehyde in PBS. For F-actin labeling, cells were permeabilized with 0.1% Triton X-100/PBS and stained for 30 min with 1 μg/ml TRITC-conjugated phalloidin (Sigma). The intensity of phalloidin fluorescence was measured using a Northern Eclipse program (Toronto). The intensity of the entire spine head (ranging from 0.3–1.0 μm in diameter) was measured and subtracted (or divided to obtain spine/dendrite ratio) by that of an adjacent dendritic area of a similar size below the neck. For immunostaining, fixed cells were permeabilized for 10 min with cold methanol, blocked for 1 hr with 1% milk/2% BSA, and then incubated with appropriate primary and then secondary antibodies. Fluorescent images were collected on a confocal microscope. The primary antibodies used were: anti-LIMK-1 (Wang et al., 1998), anti-LIMK-2 (Santa Cruz), anti-MAP2 (Upstates), anti-actin (Sigma), anti-cofilin (Santa Cruz), anti-NMDAR1 and anti-NMDAR2A/B (Upstates), anti-GluR1 (Upstates), anti-PKCα, β, γ (Sigma), anti-synapsin (Santa Cruz), anti-PAK-α, anti-PAK-β, anti-ROCK-2 (Santa Cruz), and anti-CaMKIIα (gift of Dr. Bill Trimble).

Cofilin Phosphorylation Assay

We used whole-brain slices, prepared and maintained as described for electrophysiological recordings, to analyze ADF/cofilin phosphorylation, using rabbit polyclonal antibodies specific for ADF/cofilin or phosphorylated ADF/cofilin (Meberg et al., 1998) or cofilin (Santa Cruz). The health of the slices was verified by normal synaptic responses. Under these conditions, the level of both p-AC and total cofilin remained stable for at least 3 hr. PDBu, NMDA, and glutamate were prepared in DMSO as stock solutions and added directly to the slices held in a chamber containing 2–5 ml of 95% O_2/5% CO_2-saturated extracellular solution. The treatment was terminated by homogenizing the slices at 4°C. The total protein concentration of each sample was determined and analyzed with Western blots. The amounts of cofilin and p-AC were compared by the enhanced chemiluminescence (Amersham) method of detection and the films scanned for optical density and statistical analysis.

Electrophysiology

The procedures for electrophysiological recordings were described previously (Jia et al., 1996). For LTP studies, the age of mice ranged from 2 to 6 months and, for LTD and whole-cell patch clamping, from 2 to 4 weeks. Extracellular solution contained (in mM): 120 NaCl, 2.5 KCl, 1.3 $MgSO_4$, 1.0 NaH_2PO_4, 26 $NaHCO_3$, 2.5 $CaCl_2$, and 11 D-glucose. For field EPSPs, the recording pipette (3 MOhm) was filled with extracellular solution. For whole-cell voltage clamp recordings, the patch pipette (3–5 MOhm) contained the following (in mM): 132 Cs gluconate, 17.5 CsCl, 0.05 EGTA, 10 HEPES, 2 Mg-ATP, 0.2 Na-GTP, QX-314 (pH 7.4) (292 mOsm). All data acquisition and analysis were done using pCLAMP 7 software (Axon instruments). When average data were plotted, data were normalized to the average of the baseline responses unless indicated otherwise. All data were statistically evaluated by Student's t test.

Behavioral Tests

The apparatus and definitions of recorded behaviors for open-field test were given previously (Janus et al., 1995; Jia et al., 1996). Mice were individually tested for a 5 min session per day during 2 consecutive days. The training and testing procedures and statistical analyses for fear conditioning and water maze test were described previously (Lu et al., 1997). The learning acquisition training, in which a hidden platform was always in the NE quadrant of the tank, lasted for 5 days with four trials per day (intertrial intervals of 30 min). On the sixth day, mice were given only a probe trial. The learning reversal training, in which the submerged platform was moved to the opposite (SE) quadrant, started on day 8 and lasted for 4 days followed by a probe trial 24 hr later. Only the data on swim path was reported. Other measures, including escape latency, the percentage of the path length spent by mice in the target quadrant, and thigmotaxic behavior were also analyzed, and the results were consistent with those on the swim path.

Acknowledgments

We are indebted to J. Hwang and C. Ackerley for electron microscopy assistance and to W. Abramow-Newerly and J. Roder for providing us with the R1 ES cell line. We thank L. Shen and W. Ju for assistance with Western blot analysis and J. Henderson for suggestions and assistance with neuroanatomy. We are grateful to Dr. J.R. Bamburg for supplying us with the anti-p-AC and anti-AC antibodies and to Dr. K. Misuno for providing the LIMK-1 cDNA and antibodies. This work was supported by grants from Canadian Institutes of Health Research to Z.J., grants from the NIH to D.L.F., a CIHR New Investigator Award to Z.J., and The Hospital For Sick Children Foundation (Z.J.).

Received: October 23, 2001
Revised: April 23, 2002

References

Arber, S., Barbayannis, F., Hanser, H., Schneider, C., Stanyon, C., Bernard, O., and Caroni, P. (1998). Regulation of actin dynamics through phosphorylation of cofilin by LIM kinase. Nature *393*, 805–809.

Bamburg, J.R. (1999). Proteins of the ADF/cofilin family: essential regulators of actin dynamics. Annu. Rev. Cell Dev. Biol. *15*, 185–230.

Bamburg, J.R., and Bray, D. (1987). Distribution and cellular localization of actin depolymerizing factor. J. Cell Biol. *105*, 2817–2825.

Belluji, U., Lichtenberger, L., Galaburda, A., and Korenberg, J.R. (1999). Bridging cognition, the brain and molecular genetics: evidence from Williams syndrome. Trends Neurosci. *22*, 197–207.

Bernard, O., Ganiatsas, S., Kannourakis, G., and Dringen, R. (1994). Kiz-1, a protein with LIM zinc finger and kinase domains, is expressed mainly in neurons. Cell Growth Diff. *5*, 1159–1171.

Bliss, T.V.P., and Collingridge, G.L. (1993). A synaptic model of memory: long-term potentiation in the hippocampus. Nature *361*, 31–39.

Carlier, M.F., Ressad, F., and Pantaloni, D. (1999). Control of actin dynamics in cell motility. Role of ADF/cofilin. J. Biol. Chem. *274*, 33827–33830.

Cole, J.C., Villa, B.R.S., and Wilkinson, R.S. (2000). Disruption of actin impedes transmitter release in snake motor terminals. J. Physiol. *525*, 579–586.

Comery, T.A., Harris, J.B., Willems, P.J., Oostra, B.A., Irwin, S.A., Weiler, I.J., and Greenough, W.T. (1997). Abnormal dendritic spines in fragile X knockout mice: maturation and pruning deficits. Proc. Natl. Acad. Sci. USA *95*, 5401–5404.

Edwards, D.C., Sanders, L.C., Bokoch, G.M., and Gill, G.N. (1999). Activation of LIM-kinase by Pak1 couples Rac/Cdc42 GTPase signaling to actin cytoskeletal dynamics. Nat. Cell Biol. *1*, 253–259.

Ehlers, M.D. (2002). Molecular morphogens for dendritic spines. Trends Neurosci. *25*, 64–67.

Finch, D.M., and Jackson, M.B. (1990). Presynaptic enhancement of synaptic transmission in hippocampal cell cultures by phorbol esters. Brain Res. *518*, 269–273.

Frangiskakis, J.M., Ewart, A., Morris, C., Mervis, C., Bertrand, J., Robinson, B., Klei, B., Ensing, G., Everett, L., Green, E., et al. (1996). LIM-kinase 1 hemizygosity implicated in impaired visuospatial constructive cognition. Cell *86*, 59–69.

Hall, A. (1998). Rho GTPases and the actin cytoskeleton. Science *279*, 509–514.

Harris, K.M. (1999). Structure, development, and plasticity of dendritic spines. Curr. Opin. Neurobiol. *9*, 343–348.

Janus, C., Koperwas, J.S., Janus, M., and Roder, J. (1995). Rearing environment and radial maze exploration in mice. Behav. Processes *34*, 129–140.

Jia, Z.P., Agopyan, N., Miu, P., Xiong, Z., Henderson, J., Gerlai, R., Taverna, F., Velumian, A., MacDonald, J., Carlen, P., et al. (1996). Enhanced LTP in mice deficient in the AMPA receptor, GluR2. Neuron *17*, 945–956.

Kim, C.H., and Lisman, J.E. (1999). A role of actin filaments in synaptic transmission and long-term potentiation. J. Neurosci. *19*, 4314–4324.

Kirov, S.A., Sorra, K.E., and Harris, K.M. (1999). Slices have more synapses than perfusion-fixed hippocampus from both young and mature rats. J. Neurosci. *19*, 2876–2886.

Krucker, T., Siggins, G.R., and Halpain, S. (2000). Dynamic actin filaments are required for stable long-term potentiation (LTP) in area CA1 of hippocampus. Proc. Natl. Acad. Sci. USA *97*, 6856–6861.

Krupp, J.J., Vissel, B., Thomas, C., Heinemann, S.F., and Westbrook, G.L. (1999). Interactions of calmodulin and α-actinin with the NR1 subunit modulate Ca^{2+}-dependent inactivation of NMDA receptors. J. Neurosci. *19*, 1165–1178.

Kuroda, S., Tokunaga, C., Kiyohara, Y., Higuch, O., Konishi, H., Mizono, K., Gill, G., and Kikkawa, U. (1996). Protein-protein interaction of zinc finger LIM domain with protein kinase C. J. Biol. Chem. *271*, 31029–31032.

Kuromi, H., and Kidokoro, R. (1998). Two distinct pools of synaptic vesicles in single presynaptic boutons in a temperature-sensitive Drosophila mutant, *shibire*. Neuron *20*, 917–925.

Landis, D.M., Hall, A.K., Weinstein, L.A., and Reese, T.S. (1988). The organization of cytoplasm at the presynaptic active zone of central nervous system synapse. Neuron *1*, 201–209.

Lian, J.P., Marks, P.G., Wang, J.Y., Falls, D.L., and Badwey, J.A. (2000). A protein kinase from neutrophils that specifically recognizes Ser-3 in cofilin. J. Biol. Chem. *275*, 2869–2876.

Lu, Y.M., Jia, Z.P., Janus, C., Henderson, J., Gerlai, R., Wojtowicz, M., and Roder, J. (1997). Mice lacking metabotropic glutamate receptor 5 show impaired learning and reduced CA1 long-term potentiation but normal CA3 LTP. J. Neurosci. *17*, 5196–5205.

Luo, L., Hensch, T.K., Ackerman, L., Barbel, S., Jan, L.Y., and Jan, Y.N. (1996). Differential effects of the Rac GTPases on Purkinje cell axons and dendritic trunks and spines. Nature *379*, 837–840.

Maekawa, M., Ishizaki, T., Boku, S., Watanabe, N., Fujita, A., Iwamatsu, A., Obinata, T., Ohashi, K., Mizuno, K., and Narumiya, S. (1999). Signaling from Rho to the actin cytoskeleton through protein kinases ROCK and LIM-kinase. Science *285*, 895–898.

Malenka, R.C., and Nicoll, R.A. (1999). Long-term potentiation-a decade of progress? Science *285*, 1870–1874.

Malenka, R.C., Madison, D.V., Andrade, R., and Nicoll, R.A. (1986). Potentiation of synaptic transmission in the hippocampus by phorbol esters. Nature *321*, 175–177.

Matus, A. (2000). Actin-based plasticity in dendritic spines. Science *290*, 754–758.

Meberg, P.J., Ono, S., Minamide, L.S., Takahashi, M., and Bamburg, J.R. (1998). Actin depolymerizing factor and cofilin phosphorylation dynamics: response to signals that regulate neurite extension. Cell Motil. Cytoskeleton *39*, 172–190.

Minamide, L.S., Striegl, A.M., Boyle, J.A., Meberg, P.J., and Bamburg, J.R. (2000). Neurodegenerative stimuli induce persistent ADF/cofilin-actin rods that disrupt distal neurite function. Nat. Cell Biol. *2*, 628–636.

Mitchison, T.J., and Cramer, L.P. (1996). Actin-based cell motility and cell locomotion. Cell *84*, 371–379.

Mizuno, K., Okano, I., Ohashi, K., Nunoue, K., Kuma, K., Miyata, T., and Nakamura, T. (1994). Identification of a human cDNA encoding a novel protein kinase with two repeats of the LIM/double zinc finger motif. Oncogene *9*, 1605–1612.

Morales, M., Colicos, M.A., and Goda, Y. (2000). Actin-dependent regulation of neurotransmitter release at central synapses. Neuron *27*, 539–550.

Mori, T., Okano, I., Mizuno, K., Tohyama, M., and Wanaka, A. (1997). Comparison of tissue distribution of two novel serine/threonine kinase genes containing the LIM motif (LIMK-1 and LIMK-2) in the developing rat. Mol. Brain Res. *45*, 247–254.

Morris, R., Bannerman, D., and Good, M.A. (1996). NMDA receptors and spatial learning: differential pretraining dissociates the behavioral effects of the receptor antagonist AP5 and selective hippocampal lesions. In The Hippocampus: Function and Clinical Relevance, N. Kata, ed. (New York: Elsevier), pp. 55–73.

Nakayama, A.Y., and Luo, L. (2000). Intracellular signaling pathways that regulate dendritic morphogenesis. Hippocampus *10*, 582–586.

Nakayama, A.Y., Harms, M.B., and Luo, L. (2000). Small GTPases Rac and Rho in the maintenance of dendritic spines in the hippocampal pyramidal neurons. J. Neurosci. *20*, 5329–5338.

Nimchinsky, E.A., Oberlander, A.M., and Svoboda, K. (2001). Abnormal development of dendritic spines in FMR1 knockout mice. J. Neurosci. *21*, 5139–5146.

Pak, D.T.S., Yang, S., Rudolph-Correia, S., Kim, E., and Sheng, M. (2001). Regulation of dendritic spine morphology by SPAR, a PSD-95-associated rapGAP. Neuron *31*, 289–303.

Parfitt, K.D., and Madison, D, V. (1993). Phorbol esters enhance synaptic transmission by a presynaptic, calcium-dependent mechanism in rat hippocampus. J. Physiol. *471*, 245–268.

Pin, J.P., and Duvoisin, R. (1995). The metabotropic glutamate receptors: structure and functions. Neuropharmacology *34*, 1–26.

Proschel, C., Blouin, M.J., Gutowski, N.J., Ludwig, R., and Nobel, M. (1995). Limk 1 is predominantly expressed in neural tissues and phosphorylates serine, threonine and tyrosine residues in vitro. Oncogene *11*, 1271–1281.

Rao, A., and Craig, A.M. (2000). Signaling between the actin cytoskeleton and the postsynaptic density of dendritic spines. Hippocampus *10*, 527–541.

Rosenmund, C., and Westbrook, G.L. (1993). Calcium-induced actin depolymerization reduces NMDA channel activity. Neuron *10*, 805–814.

Sala, C., Piech, V., Wilson, N.R., Passafaro, M., Liu, G., and Sheng, M. (2001). Regulation of dendritic spine morphology and synaptic function by Shank and Homer. Neuron *31*, 115–130.

Smart, F.M., and Halpain, S. (2000). Regulation of dendritic spine stability. Hippocampus *10*, 542–554.

Smolich, B., Mynga, V., Buckely, S., Plowan, G., and Papkoff, J. (1997). Cloning and biochemical characterization of LIMK-2, a protein kinase containing two LIM domains. J. Biochem. *121*, 382–388.

Sorra, K.E., and Harris, K.M. (2000). Overview on the structure, composition, function, development, and plasticity of hippocampal dendritic spines. Hippocampus *10*, 501–511.

Sumi, T., Matsumoto, K., Takai, Y., and Nakamura, T. (1999). Cofilin phosphorylation and actin cytoskeletal dynamics regulated by Rho- and Cdc42-activated LIM-kinase 2. J. Cell Biol. *147*, 1519–1532.

Sumi, T., Matsumoto, K., and Nakamura, T. (2001). Specific activation of LIM kinase 2 via phosphorylation of threonine 505 by ROCK, a Rho-dependent protein kinase. J. Biol. Chem. *5*, 670–676.

Toshima, J., Toshima, J.Y., Amano, T., Yang, N., Narumiya, S., and Mizuno, K. (2001). Cofilin phosphorylation by protein kinase testicular protein kinase 1 and its role in integrin-mediated actin reorganization and focal adhesion formation. Mol. Biol. Cell *12*, 1131–1145.

Wang, J.Y., Frenzel, K.E., Wen, D., and Falls, D.L. (1998). Transmembrane neuregulins interact with LIM kinase *1*, a cytoplasmic protein kinase implicated in development of visuospatial cognition. J. Biol. Chem. *273*, 20525–20534.

Wang, J.Y., Wigston, D.J., Rees, H.D., Levey, A.I., and Falls, D.L. (2000). LIM kinase 1 accumulates in presynaptic terminals during synapse maturation. J. Comp. Neurol. *416*, 319–334.

Wyszynski, M., Lin, J., Rao, A., Nigh, E., Beggs, A.H., Craig, A.M., and Sheng, M. (1997). Competitive binding of α-actinin and calmodulin to the NMDA receptor. Nature *385*, 439–442.

Yang, N., Higuchi, O., Ohashi, K., Nagata, K., Wada, A., Kangawa, K., Nishida, E., and Mizuno, K. (1998). Cofilin phosphorylation by LIM-kinase 1 and its role in Rac-mediated actin reorganization. Nature *393*, 809–812.

Yuste, R., Majewaska, A., and Holthoff, K. (2000). From form to function: calcium compartmentalization in dendritic spines. Nat. Neurosci. *3*, 653–659.

Zhou, Q., Xiao, M.Y., and Nicoll, R.A. (2001). Contribution of cytoskeleton to the internalization of AMPA receptors. Proc. Natl. Acad. Sci. USA *98*, 1261–1266.